

Electrostatic Self-Assembly Deposition of Titanate(IV) Layered Oxides Intercalated with Transition Metal Complexes and Their Electrochemical Properties

Ugur Unal, Yasumichi Matsumoto,* Noriyuki Tanaka, Yoshitaka Kimura, and Naoko Tamoto

Department of Applied Chemistry, Faculty of Engineering, Kumamoto University, Kurokami 2-39-1, Kumamoto 860-8555, Japan

Received: August 4, 2003; In Final Form: September 5, 2003

The electrostatic self-assembly deposition (ESD) of the titanate layered oxides intercalated with some transition metal complexes, their phase changes with heat treatment, and their electrochemical properties have been demonstrated. The ESD occurred when both the solutions containing the complex cations with positive charge and the exfoliated Ti–O nanosheets with negative charge were mixed at an appropriate pH. The resulting deposits were the intercalated titanate oxides with a single-phase layered crystal structure in (0k0) orientation. The hexaammine complex intercalated samples possessed a layer distance of ~ 11.5 Å, whereas the $\text{Ru}(\text{bpy})_3^{2+}$ intercalated one had a layer distance of 16.6 Å. The heat-induced phase change and thermal behavior of the films depending on the intercalated complexes were discussed on the basis of various thermogravimetric differential thermal analysis (TG/DTA), X-ray diffraction analysis (XRD), and X-ray photoelectron spectroscopy (XPS) data. In the case of $\text{Ru}(\text{bpy})_3^{2+}$ intercalated sample, the heat treatment at 300 °C resulted in the strong combination of the complex with the Ti–O host layers and then brought about the visible light photocurrents. In general, the intercalated transition metal complex cations acted as the recombination center for the electron and hole produced in the host Ti–O layers under UV illumination. The $\text{Ag}(\text{NH}_3)_2^+$ intercalated in the interlayer showed a clear redox electrochemical reaction in which fine Ag metal particulates were produced by the electrochemical reduction. The mechanisms of the electrochemical and photoelectrochemical properties of the intercalated Ti–O oxides are discussed in detail on the basis of the interaction between the intercalated complexes and the Ti–O host layers, as well as their energy positions.

Introduction

Compounds with a layered structure have interesting chemical properties that largely change with the intercalation,^{1–8} ion exchange,^{9–16} and pillaring^{17–22} into the interlayer. The properties are also highly dependent on the kind of cation or molecule being intercalated. These types of layered materials have some applications in the fields of photocatalysis,^{23–29} photoluminescence,^{30–34} and photoelectrochemistry.^{35,36} In general, semiconducting layered oxides consisting of Ti, Ta, and Nb possess a high photocatalytic activity for the photodecomposition of water^{23–26} and act as an n-type semiconductor.^{35,36} Intercalated molecules such as water and some organics are very active in photoreaction and are easily decomposed by the electron–hole pair produced in the $\text{M}_1\text{–O}$ ($\text{M}_1 = \text{Ti}, \text{Nb}, \text{and Ta}$) host layer under illumination of UV light with energies larger than the band gap of the host layers.^{37,38}

Some stable intercalated cations and molecules will act as an electron donor, an acceptor, or a recombination center due to their energy levels with respect to the host layers and may bring about drastic changes in physical or chemical properties or both. It is very important for the development of new photocatalysts and electrodes in photocells to know the effects of the stable intercalated species on the electrochemical and photoelectrochemical properties. Moreover, some energy levels vs solution can sometimes be derived from these properties, which are very useful when discussing the mechanism in the photocatalysis and other devices using an electron transfer.

However, the electrochemical and photoelectrochemical behavior of the $\text{M}_1\text{–O}$ layered oxides intercalated with stable cations such as transition metals and metal complexes has yet to be studied.

The intercalation of cations or molecules into the $\text{M}_1\text{–O}$ layered oxides has mainly been performed on the basis of the ion-exchange principles by treating the oxide with the solution including the cations of interest. In general, the ion-exchange reaction has been carried out between the protons in the protonated titanate or the large size ammonium ions such as tetrabutylammonium (TBA) intercalated in advance and other cations. This method, however, is a time-wasting process and sometimes results in only partial ion exchange. Therefore, a new method should be developed for the preparation of $\text{M}_1\text{–O}$ layered oxides intercalated completely and easily to study the effects of the intercalated species on their electrochemical properties.

In this paper, at first we demonstrate a new technique to prepare the intercalated Ti–O layered oxides, in which electrostatic self-assembly deposition (ESD) takes place. This technique is based on the electrostatic combination of the Ti–O nanosheets with negative charge and cations after mixing the colloidal solution of Ti–O nanosheets with the solution containing cations. Second, phase changes of the intercalated samples by heat treatment are presented, and the interaction of the intercalated cations with the Ti–O host layers is discussed. Third, we demonstrate some unique electrochemical and photoelectrochemical properties of the Ti–O layered oxides intercalated with transition metal complex cations and discuss their

* Corresponding author. E-mail: yasumi@gpo.kumamoto-u.ac.jp. Tel: +81-96-342-3658. Fax: +81-96-342-3679.

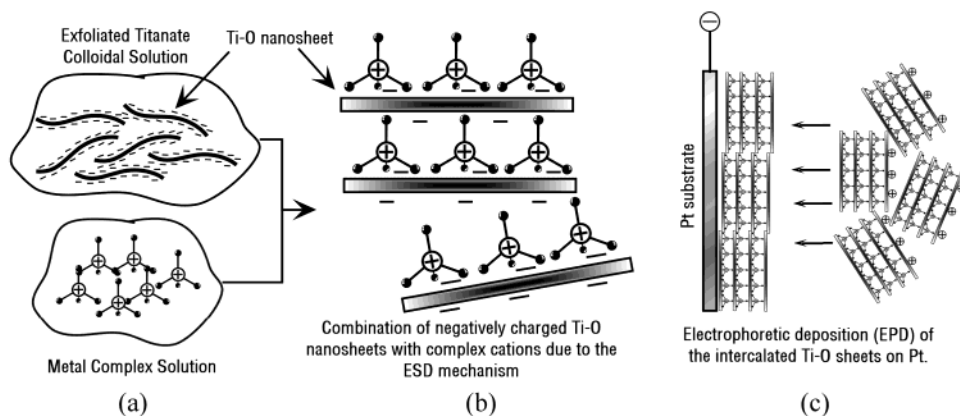


Figure 1. The pictorial view of the ESD and EPD mechanisms.

mechanisms in terms of the interaction between the complexes and the Ti–O host layers, as well as their energy positions.

Experimental Section

$\text{Cs}_x\text{Ti}_{(2-x/4)}\square_{x/4}\text{O}_4$ (C–Ti oxide) as the starting material was prepared by the complex polymerization method.³⁵ Prior to the addition of $\text{Ti}(\text{OCH}(\text{CH}_3)_2)_4$ (10.8 mL), Cs_2CO_3 (3.50 g) was dissolved in a mixture of methanol (160 mL) and ethylene glycol (60 mL). During the addition of titanium isopropoxide, the mixture was stirred vigorously with a magnetic stirrer and the temperature was raised gradually to 50 °C. The resultant solution was clear. Next, anhydrous citric acid (28.8 g) was added, and the temperature was raised to 150 °C, yielding a resin-like mass, which was transformed into ash and then into white powder upon raising the temperature to 300 °C. Calcination of the powder at 800 °C yielded the final C–Ti oxide ($\text{Cs}_x\text{Ti}_{(2-x/4)}\square_{x/4}\text{O}_4$, where $x = 0.76$ because Cs/Ti was measured to be 0.42 by X-ray photoelectron spectroscopy (XPS) analysis) product. Consequently, all Ti cations in the present C–Ti oxide exist as Ti^{4+} . The final product of the C–Ti oxide powder was pulverized in a ball mill in various solutions such as acetone, methanol, and ethanol to form a powder with fine particles. The average particle size was about 1–4 μm after milling. Protonation of this product resulted in $\text{H}_x\text{Ti}_{(2-x/4)}\square_{x/4}\text{O}_4 \cdot \text{H}_2\text{O}$ (H–Ti oxide). Protonation was performed by stirring 5 g of C–Ti oxide powder in 200 mL of 1 M aqueous HCl solution for 24 h. In fact, this sample contained only a small amount of Cs (Cs/Ti atomic ratio < 0.04). The H–Ti oxide powder was obtained by subsequent vacuum filtration.

The exfoliation of the powders was performed by treating the H–Ti oxide powder with an ethylamine solution for 24 h. The subsequent centrifugation under 2000 rpm for 30 min yielded colloidal suspensions of exfoliated Ti–O nanosheets. Ten milliliters of the ethylamine-exfoliated colloidal solution was mixed with 0.01 M metal-complex solutions to obtain metal-complex intercalated Ti–O layered structures. The metal-complex solutions were prepared by dissolving the metal-complex salts in pH 8.5 $\text{NH}_3/\text{NH}_4^+$ buffer solution to control the pH to avoid possible metal-hydroxide formation. By extraction from the titration curves, we have chosen the optimum pH as 8.5 to prepare the intercalation solution because the exfoliated Ti–O sols were also stable in the pH range of 5.5–12. In the case of the preparation of the $\text{Ag}(\text{NH}_3)_2^+$ intercalated sample, $\text{Ag}(\text{NH}_3)_2^+$ solution was prepared by solving its Cl^- salt in water by adding an excess amount of concentrated ammonium solution until the salt dissolved completely (pH = 11 ± 0.5). When the negatively charged Ti–O nanosheets suspended in the solution come in contact with the $\text{M}(\text{NH}_3)_x^{y+}$

cations, they combine because of the electrostatic self-assembly deposition (ESD) mechanism to result in precipitates. The precipitate consists of single-phase Ti–O layered oxide intercalated with metal-complex cations. The precipitates were washed first with water and then acetone to remove the excess ions. Following the washing process, the intercalated Ti–O layered oxide was deposited on a Pt electrode electrophoretically by applying 10 V for 10 min in acetone/ I_2 solution (EPD technique). The experimental overview and the mechanism are illustrated in Figure 1. However, the present EPD technique was not suitable for the deposition of the Ti–O layered oxides intercalated with $\text{Ag}(\text{NH}_3)_2^+$ because of the reaction between Ag^+ and I^- . Consequently, the deposits of the $\text{Ag}(\text{NH}_3)_2^+$ intercalated Ti–O sheets were pasted on the Pt substrate and then treated with subsequent drying at room temperature.

The Ti–O layered oxides intercalated with $\text{Ru}(\text{bpy})_3^{2+}$ were prepared by the following procedure: In this case, a TBA (tetrabutylammonium)-exfoliated Ti–O nanosheet solution was used instead, which was prepared using the same method as for the ethylamine exfoliation. Prior to the addition of a certain amount of the above Ti–O exfoliated solution into the 20 mL of 1 mM $\text{Ru}(\text{bpy})_3^{2+}$ solution with a pH value of 6, pH of the TBA-exfoliated Ti–O was adjusted to 7 with 0.1 M HCl. The Ru/Ti ratio was 1 after the addition, and the subsequent precipitation occurred instantly because of the ESD mechanism. The precipitate was washed with water and then pasted on the InO_2 or Pt substrate.

The morphology of the deposited films was observed by SEM. The crystal structure and the orientation were analyzed from X-ray diffraction analysis (XRD) patterns (using Cu K α radiation, Rigaku RINT-2500VHF). The compositions of the deposited films were analyzed using an inductively coupled plasma (ICP) spectrophotometer (Nippon Jarrell Ash IRIS Advantage) and an X-ray photoelectron spectrometer (XPS, VG Scientific Σ -probe). The ICP was carried out after dissolving the films in HCl solution. Infrared spectra of the films were obtained with an attenuated total reflection–Fourier-transform infrared (ATR/FTIR) spectrometer (Nicolet 560). UV–vis absorption spectra of the deposited oxides were measured using an UV–vis spectrometer (Jasco V-550). Thermogravimetric differential thermal analysis (TG/DTA) curves were obtained by thermal analysis (Seiko TG/DTA).

All electrochemical experiments were carried out in a conventional three-electrode electrochemical cell with a Pt counter electrode and a saturated Ag/AgCl reference electrode. The working electrode potentials were referred to this reference electrode unless otherwise stated in this paper. A 500 W ultrahigh-pressure Hg lamp was used as the light source to

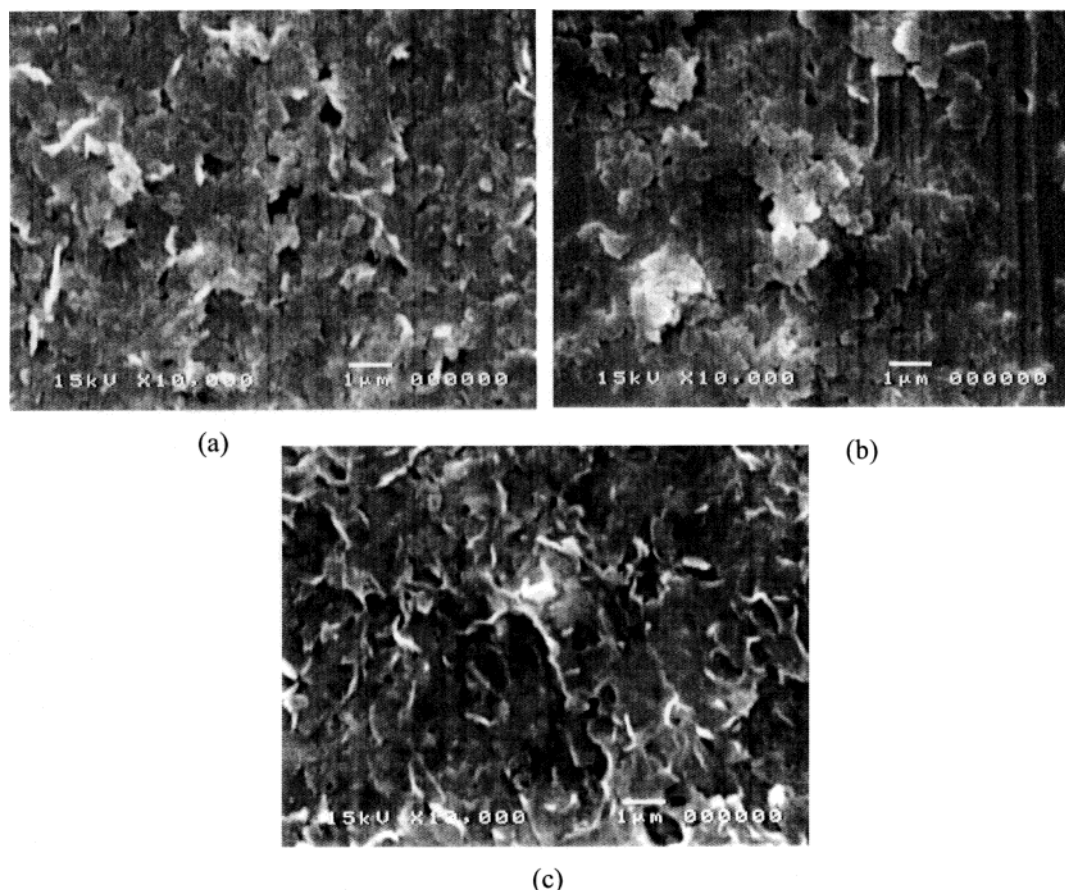


Figure 2. The SEM micrographs of the deposited Ti–O layered oxides intercalated with metal complexes prepared by the ESD technique: (a) EPD film of the Ti–O sheet intercalated with $\text{Ru}(\text{NH}_3)_6^{3+}$; (b) pasted film of the Ti–O sheet intercalated with $\text{Ag}(\text{NH}_3)_2^+$; (c) pasted film of the Ti–O sheet intercalated with $\text{Ru}(\text{bpy})_3^{2+}$.

measure the photoelectrochemical properties. Cyclic voltammograms (CV) were measured under potential sweep rate of 20 mV s^{-1} . A $0.1 \text{ M K}_2\text{SO}_4$ solution was used as a supporting electrolyte solution. The electrolytes were saturated with N_2 prior to the electrochemical measurements.

Results and Discussion

Preparation of the Intercalated Ti–O Layered Oxides by the ESD Technique. The model of the ESD mechanism is depicted in Figure 1b. The addition of the exfoliated Ti–O nanosheet colloidal solution into the aqueous solution containing metal complexes (Figure 1a) resulted in the formation of the Ti–O layered oxides intercalated with the metal complex cations due to the electrostatic principles governing the deposition (Figure 1b). The ESD occurred immediately after the colloidal solution was added to the solution. The pH of the aqueous solutions of metal complexes was in the range of 4.5–5, whereas the pH of the Ti–O colloidal solution was around 11.5. The addition of the Ti–O colloidal solution into the aqueous solutions of some metal complexes without any pH adjustment resulted in metal hydroxide formations due to the high pH of the colloidal solution. In addition, at pH values lower than 5, the exfoliated titanate sheets were precipitated because of the intercalation of H^+ or H_3O^+ or both into the interlayer. On the other hand, Ni^{2+} and Ru^{2+} hexaammine complexes could only be dissolved in ammonium environments even at high pH values. Consequently, $\text{NH}_3/\text{NH}_4^+$ buffer solution was used to keep the pH at 8.5 at which only the ESD occurred without any hydroxide formation.

Figure 2 shows the microphotographs of the surface of the deposited films of the Ti–O sheets intercalated with metal

complexes on the Pt substrate. The mosaic-like pattern of the surface was constructed by the EPD of the intercalated Ti–O sheets onto the Pt substrate (Figure 1c). As it can be seen from the micrographs, each sheet can be easily distinguished, and their size is virtually uniform, around $1 \mu\text{m}$ in its planar surface and about $0.1 \mu\text{m}$ in its thickness. Consequently, an intercalated sheet is formed from approximately 10 units of piled up Ti–O nanosheets. The orientation of the intercalated Ti–O sheets was parallel to the substrate surface. In addition, the surface of the electrophoretically deposited films (Figure 2a) was relatively smoother than those of the pasted films (Figure 2b,c).

In the FTIR spectra of all of the films intercalated with ammine complex cations, two intense peaks at 1340 and 1640 cm^{-1} (see Supporting Information, Figure S1), which are assigned to the symmetrical and asymmetrical bending modes of the coordinated NH_3 in the complex, respectively,³⁹ were observed. In the case of the $\text{Ru}(\text{bpy})_3^{2+}$ intercalated film, the pyridine ring stretching peaks of 1420 and 1602 cm^{-1} were observed and the 1300 – 1700 cm^{-1} fingerprint region of a $\text{Ru}(\text{bpy})_3^{2+}$ complex possessed the peaks belonging to the complex (see Supporting Information, Figure S2).⁴⁰ The nitrogen/metal ratio calculated from the XPS spectra of the films intercalated with ammine complexes corresponded to the ratio in the complexes (N/M atomic ratios were about 6 and 2 for $\text{M}(\text{NH}_3)_6^{n+}$ and $\text{M}(\text{NH}_3)_2^{m+}$, respectively), meaning that NH_4^+ or ethylamine or both from the solutions scarcely coexist in the interlayer. Thus, each complex cation was easily intercalated in each sample prepared by the ESD technique.

The XRD diffraction patterns of the Ti–O sheet films intercalated with metal complexes are shown in Figure 3. All of the samples consisted of a highly crystalline layered single

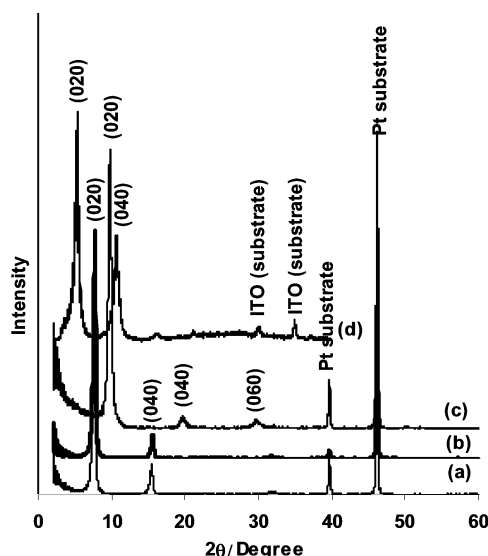


Figure 3. XRD patterns of some Ti-O layered oxides intercalated with metal complex cations: (a) $\text{Ru}(\text{NH}_3)_6^{3+}$ -TiO; (b) $\text{Co}(\text{NH}_3)_6^{3+}$ -TiO; (c) $\text{Ag}(\text{NH}_3)_2^+$ -TiO; (d) $\text{Ru}(\text{bpy})_3^{2+}$ -TiO.

TABLE 1: Layer Distances and Atomic Ratios of the Complex Intercalated Ti-O Films

intercalated metal complex	layer distance (Å)	M/Ti atomic ratio	composition ^a
$\text{Co}(\text{NH}_3)_6^{3+}$	11.41	0.12	$[\text{Co}(\text{NH}_3)_6^{3+}]_{0.22}\text{Ti}_{1.81}\text{O}_4 \cdot 2.4\text{H}_2\text{O}$
$\text{Ru}(\text{NH}_3)_6^{3+}$	11.47	0.22	$[\text{Ru}(\text{NH}_3)_6^{3+}]_{0.19}\text{Ti}_{1.81}\text{O}_4 \cdot 2.1\text{H}_2\text{O}$
$\text{Ru}(\text{NH}_3)_6^{2+}$	11.53	0.16	$[\text{Ru}(\text{NH}_3)_6^{2+}]_{0.13}\text{Ti}_{1.81}\text{O}_4 \cdot 4.2\text{H}_2\text{O}$
$\text{Ni}(\text{NH}_3)_6^{2+}$	11.41	0.46	$[\text{Ni}(\text{NH}_3)_6^{2+}]_{0.68}\text{Ti}_{1.81}\text{O}_4 \cdot 2.9\text{H}_2\text{O}$
$\text{Ag}(\text{NH}_3)_2^+$	8.99	0.4	$[\text{Ag}(\text{NH}_3)_2^+]_{0.32}\text{Ti}_{1.81}\text{O}_4 \cdot 0.7\text{H}_2\text{O}$
$\text{Ru}(\text{bpy})_3^{2+}$	16.6	0.04	$[\text{Ru}(\text{bpy})_3^{2+}]_{0.07}\text{Ti}_{1.81}\text{O}_4 \cdot 2.5\text{H}_2\text{O}$

^a The compositions were calculated from the atomic ratio (ICP and XPS) and water content (TG/DTA).

phase oriented in the (0k0) direction. The hexaammine complexes (e.g., $\text{Ru}(\text{NH}_3)_6^{3+}$, $\text{Co}(\text{NH}_3)_6^{3+}$) had a layer distance around 11.4 Å, whereas that of the $\text{Ru}(\text{bpy})_3^{2+}$ was 16.6 Å because of the larger molecular size. On the other hand, the layer distance was relatively small for the $\text{Ag}(\text{NH}_3)_2^+$ intercalated sample because of its linear structure and its orientation in the interlayer. The layer distances of all of the intercalated Ti-O films were tabulated in Table 1. Water content of each film was calculated from the thermal analysis data as stated in the later section. The atomic ratios of M/Ti in the compound, where M stands for the metals in the complexes, were determined from the ICP or XPS analyses or both. The calculated compositions of the intercalated Ti-O films are also listed in Table 1. The original $\text{Cs}_{0.76}\text{Ti}_{1.81}\text{O}_4$ powder suggests that 1 mol of the compound requires 0.76 mol of intercalated monovalent cations in the composition to compensate the negative charge of the Ti-O layer. In the cases of Co, Ru, and Ag complex intercalated Ti-O films, the positive charge is deficient, while the positive charge is in excess in the case of Ni complex cation. Probably, H^+ , H_3O^+ or both or OH^- ions will be copresent in the interlayer to keep the charge balance because no anion such as Cl^- or ethylamine with a positive charge was observed according to the XPS.

Upon the basis of the information given above, we can construct a model of the intercalated oxides. The comparison of the layer distances with the size of the complex cations leads us to conclude that the complexes are present in the interlayer in a single-layer arrangement. Sakaki et al. reported the layer distance of the dehydrated form of the H-Ti oxide as 6.6 Å,

where the size of the interlayer protons was neglected.^{3,11} In the case of the hexaammine complex intercalated samples, the layer distances are in the range of 11.41–11.53 Å as listed in Table 1. Therefore, the interlayer distances related to the hexaammine complexes were calculated to be 4.8–4.9 Å, which are approximately equal to the molecular size of the hexaammine cations. According to the TG/DTA data, water molecules were also intercalated together with the complexes and will be located in the cavities between the complex molecules and the Ti-O layers. As for the silver complex intercalated film, the interlayer distance is 2.4 Å, which is almost half the size of the longest length of the complex cation. Thus, the complex cations will be placed in the interlayer in an inclined or a horizontal form. The possible models of the intercalated films for the hexaammine complexes and $\text{Ag}(\text{NH}_3)_2^+$ are depicted in Figure 4, panels a and b, respectively. The direct interaction between the Ag^+ in the $\text{Ag}(\text{NH}_3)_2^+$ and the host Ti-O with a negative charge will occur to some extent via the electrostatic force, while the direct interaction will be suppressed by the surrounding NH_3 ligands in the hexaammine complex cations. This brings about a difference in the electrochemical behavior as stated in a later section.

It has been reported that the change in the interlayer distance for some layered materials with respect to the basal spacing after the intercalation of $\text{Ru}(\text{bpy})_3^{2+}$ is around 9 Å, which is approximately equal to the diameter of the $\text{Ru}(\text{bpy})_3^{2+}$ ion.^{5,6,41,42} In the present study, the interlayer distance after the intercalation was 10 Å as shown in Figure 4c. The relatively large distance for the present case is ascribable to the presence of the surrounding water or hydronium ions and will give relatively weak interaction between the $\text{Ru}(\text{bpy})_3^{2+}$ and Ti-O host layer. The heat-treated samples showed a slight decrease in the interlayer distance, as will be discussed in a further section.

The representation of the planar surface through the *b* axis is also given in Figure 4, panels d and e, for the samples intercalated with hexaammine and $\text{Ru}(\text{bpy})_3^{2+}$ complexes, respectively. Assuming that the complex cation closely occupies the interlayer space, the theoretical M/Ti ratio can be estimated by taking the ratio of a complex cation to the number of Ti atoms in an area that a complex cation occupies. According to the estimation, the Ru/Ti ratio for the $\text{Ru}(\text{bpy})_3^{2+}$ intercalated Ti-O sample is approximately 0.035, which is in good agreement with the experimental results listed in Table 1. The estimation of the theoretical value for the hexaammine complex intercalated Ti-O sample yielded the value of 0.12, and that for the $\text{Ag}(\text{NH}_3)_2^+$ was 0.3. These values are close to the experimental values as listed in Table 1. Thus, the complex cations will exist in a relatively close packed formation in the interlayer, although the theoretical values include some potential errors coming from the estimation.

Heat Treatment of the Intercalated Ti-O Layered Oxides.

The TG/DTA curves of the $\text{Ru}(\text{NH}_3)_6^{3+}$ and $\text{Co}(\text{NH}_3)_6^{3+}$ complex intercalated Ti-O samples are given in Figure 5, panels a and b, respectively. In these cases, the weight loss occurred mainly in four steps for the ammine complex intercalated films. The first two weight loss regions, that is, from room temperature to about 150 °C and from 150 to about 250 °C, might be assigned to the release of the free and intercalated water, respectively. Thermal analysis of the complex compounds revealed that the weight loss of the ammine complexes by oxidation roughly started around 225 °C and ended around 500 °C. Thus, because the starting point of the weight loss of the ammine complexes overlaps with the release of the intercalated water, the amount of intercalated water was calculated from

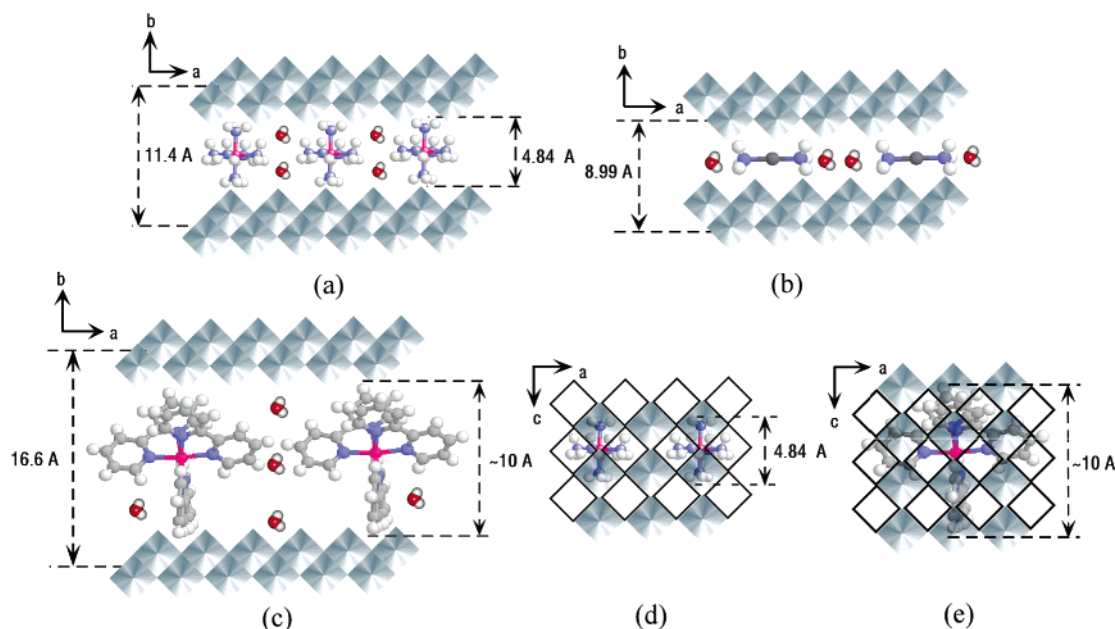


Figure 4. Pictorial view of the structure models for (a) hexaammine complex ($\text{Co}(\text{NH}_3)_6^{3+}$), (b) silver complex, and (c) $\text{Ru}(\text{bpy})_3^{2+}$ intercalated Ti—O oxides through *c*-axis and areal size models for (d) hexaammine complex ($\text{Co}(\text{NH}_3)_6^{3+}$) and (e) $\text{Ru}(\text{bpy})_3^{2+}$ intercalated Ti—O oxides through *b*-axis.

the weight loss in the range of 150 to 225 °C. The values given in Table 1, therefore, have some errors due to neglecting the potential loss of the intercalated water over 225 °C.

In Figure 5a, the first sharp exothermic peak at 300 °C and the second broad exothermic peak at 450 °C, together with the weight loss, are based on the decomposition and removal of the amines by oxidation because the N1s peak drastically decreased by the heat treatment at 400 °C and completely disappeared at 600 °C according to the XPS analysis as shown in Figure 6a. The N1s and Ru3d XPS spectra of the $\text{Ru}(\text{NH}_3)_6^{3+}$ intercalated sample at different temperatures are given in Figure 6, panels a and b, respectively. The peak at 281.0 eV for the 300 °C heat-treated sample in Figure 6b shows the presence of RuO_2 . As seen from Figure 6a, the N1s peak is still observed at 300 °C with a shift to the higher energy, suggesting that an oxidative state of N is also formed by the heat treatment at 300 °C. The reaction at 450 °C accompanies the phase change to rutile according to the XRD analysis as shown in Figure 7a. Consequently, the decomposition and release of the amines via the oxidative state bring about the destruction of the layered structure as shown in Figure 7a. The layered structure disappeared after the heat treatment at 400 °C. In the case of Figure 5b, which represents the thermal behavior of the $\text{Co}(\text{NH}_3)_6^{3+}$ intercalated Ti—O sample, the exothermic and endothermic peaks were relatively indistinguishable. In addition, the decomposition and removal of the ammine was distributed in a wider range, and the weight loss was gradual. Both the $\text{Co}(\text{NH}_3)_6^{3+}$ and $\text{Ag}(\text{NH}_3)_2^+$ intercalated samples exhibited a similar phase change to that of the $\text{Ru}(\text{NH}_3)_6^{3+}$ according to the N1s XPS spectrum and the XRD analysis (Figure 7b,c).

The changes in the XRD patterns of the $\text{Ru}(\text{NH}_3)_6^{3+}$, $\text{Co}(\text{NH}_3)_6^{3+}$, and $\text{Ag}(\text{NH}_3)_2^+$ intercalated films by heat treatment are given in Figure 7, panels a, b, and c, respectively. The heat treatment at 200 °C led to the contraction of the layer distance due to the release of the intercalated water molecules, except for the $\text{Ag}(\text{NH}_3)_2^+$ intercalated sample in which only a small amount of water molecules existed as listed in Table 1. The hexaammine complex intercalated samples all behaved in a similar manner. The layer distances decreased to 8.65 Å for the $\text{Ru}(\text{NH}_3)_6^{3+}$ and 7.47 Å for the $\text{Co}(\text{NH}_3)_6^{3+}$ intercalated

samples by the heat treatment at 200 °C. The heat treatment at 600 °C led to the formation of an anatase phase for the $\text{Co}(\text{NH}_3)_6^{3+}$ intercalated sample, while the $\text{Ru}(\text{NH}_3)_6^{3+}$ intercalated sample had a single rutile phase at 600 °C.

The $\text{Ru}(\text{bpy})_3^{2+}$ intercalated sample lost weight in three steps as seen in Figure 5c. The weight losses between room temperature and 100 °C and 120 and 240 °C can be assigned to the evaporation of the free and intercalated water, respectively. The amount of the intercalated water molecule can be easily calculated from the clear weight loss in the range of 120–240 °C. Because the decomposition of the $\text{Ru}(\text{bpy})_3^{2+}$ complex itself starts at 320 °C by oxidation, the weight loss starting around 320 °C was attributed to the decomposition of the intercalated $\text{Ru}(\text{bpy})_3^{2+}$ cations. The exothermic peak at 400 °C also denotes the decomposition of the complex cations in the interlayer by oxidation.

The N1s peak of the $\text{Ru}(\text{bpy})_3^{2+}$ intercalated sample at 400.4 eV, which belongs to the pyridine group of the complex, was broadened by the heat treatment, as seen in Figure 8a. The shoulder peak at 402.4 eV suggests the protonated pyridinic nitrogen,⁴³ which is the result of the interaction of the pyridinic nitrogen with the surrounding hydronium ions or protons, and it disappeared at 200 °C as a result of the removal of the surrounding molecules. The peak at 398.8 eV appears when the sample is heated at 300 °C. The low-energy shift of the N1s peak is presumably due to the alteration in the interaction state of the $\text{Ru}(\text{bpy})_3^{2+}$ complex with the Ti—O layers after the release of the water molecules and due to the strained configuration together with the partial decomposition of the bipyridine moieties. In contrast to the shift in the binding energy of N1s, the Ru3d peak maintained its position at 281.3 eV at 200 °C and slightly shifted to the lower energies at 300 °C (Figure 8b). By the heat treatment at 400 °C, the N1s and C1s peaks have drastically disappeared because of the decomposition of the complex molecule. Consequently, the relatively large change in the binding energy of the N1s means that the pyridine in the intercalated $\text{Ru}(\text{bpy})_3^{2+}$ interacts with the Ti—O host layers by the heat treatment at 200–300 °C.

In contrast with the ammine complex intercalated films, the $\text{Ru}(\text{bpy})_3^{2+}$ intercalated film kept its layered structure without

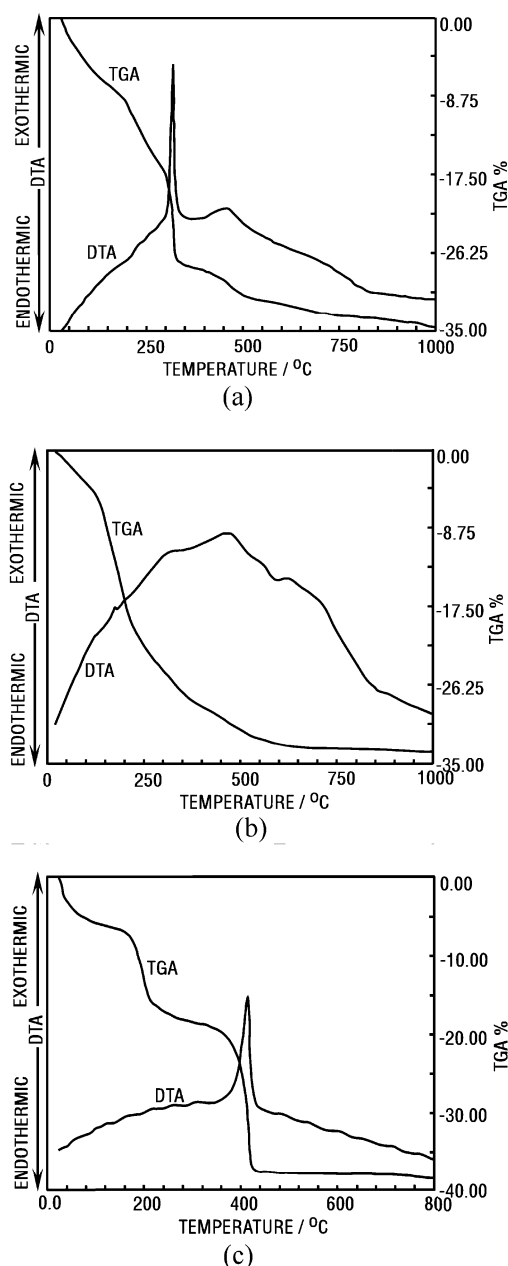


Figure 5. TG/DTA curves of (a) $\text{Ru}(\text{NH}_3)_6^{3+}$, (b) $\text{Co}(\text{NH}_3)_6^{3+}$, and (c) $\text{Ru}(\text{bpy})_3^{2+}$ intercalated Ti–O oxides

any change up to 300 °C, despite the very slight shift to a higher angle, as seen in Figure 9. The result is in harmony with the thermal behavior of the sample. The resulting interlayer distance after the heat treatment at 300 °C was 9.11 Å, which is slightly less than the diameter of $\text{Ru}(\text{bpy})_3^{2+}$. In this state, the intercalated $\text{Ru}(\text{bpy})_3^{2+}$ will interact with the Ti–O host layers as stated above. The original layer structure was destroyed by the heat treatment at temperatures higher than 400 °C, where the decomposition of $\text{Ru}(\text{bpy})_3^{2+}$ also occurs, yet the film possessed other layered structures.

The UV–vis reflectance spectra of the $\text{Ru}(\text{bpy})_3^{2+}$ intercalated sample are given in Figure 10 before and after heat treatment at different temperatures. The absorption due to the metal-to-ligand charge transfer (MLCT) of the $\text{Ru}(\text{bpy})_3^{2+}$ starting at around 590 nm for the as-prepared sample shifted to red, and the band broadened by heat treatment. The film heat-treated at 400 °C, however, showed quite a different spectrum, which is apparently related to the decomposition of the Ru–

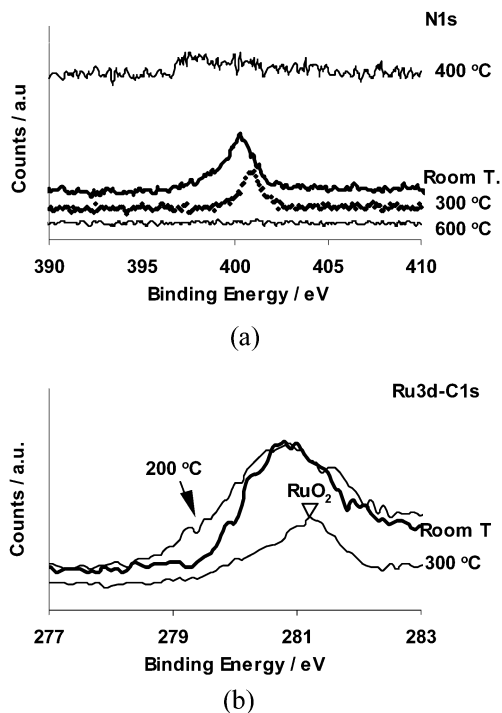


Figure 6. XPS (a) N1s and (b) Ru3d spectra of the heat-treated $\text{Ru}(\text{NH}_3)_6^{3+}$ intercalated films at different temperatures.

$(\text{bpy})_3^{2+}$ complex. The shift for the intercalated $\text{Ru}(\text{bpy})_3^{2+}$ molecules with respect to the peak for the molecule in an aqueous solution was also reported in other studies related to zeolites or layered materials,^{4–6,13,41} and it was assigned to the strained complex molecules^{4,13} and to the chelate–oxide layer and chelate–chelate interaction.⁵ To the best of our knowledge, such a large shift due to the heat treatment is the first report for the complex intercalated oxide films. Thus, the shift is ascribable to the advancement in the interaction due to the removal of the water surrounding the complex molecules by the heat treatment at 200–300 °C. The infrared spectra of the $\text{Ru}(\text{bpy})_3^{2+}$ intercalated sample was measured before and after the heat treatment. The original pyridine values in the fingerprint 1300–1700 cm^{-1} region for the sample heated at 300 °C were still observable but not for the samples heated at 400 °C. Consequently, the $\text{Ru}(\text{bpy})_3^{2+}$ cation exists together with the strong interaction of the pyridine with the Ti–O host layers in the interlayer even after the heat treatment at 300 °C.

Electrochemical Properties of the Intercalated Ti–O Layered Oxides. During the submersion of the film/substrate into the K_2SO_4 electrolyte, the intercalated complex cations with the exception of the $\text{Ag}(\text{NH}_3)_2^+$ intercalated and the heat treated $\text{Ru}(\text{bpy})_3^{2+}$ intercalated samples, slowly dissolved from the interlayer into the solution. For example, the XRD pattern of the $\text{Ru}(\text{bpy})_3^{2+}$ intercalated films taken after the submersion exhibited contraction of the layer distance from 16.6 to 9.3 Å because of the deintercalation of the $\text{Ru}(\text{bpy})_3^{2+}$ into the K_2SO_4 solution by ion exchange between the $\text{Ru}(\text{bpy})_3^{2+}$ and K^+ (the XPS analysis also confirmed the ion exchange.). The easy exchange is due to the weak interaction between the intercalated complexes and the host Ti–O layers. The $\text{Ru}(\text{bpy})_3^{2+}$ intercalated sample heat-treated at 300 °C, however, kept its single-phase layered structure without any change, even after the continuous potential sweep carried out over 2 h (see Supporting Information, Figure S3). This is based on the strong interaction between the pyridine in the intercalated $\text{Ru}(\text{bpy})_3^{2+}$ and the Ti–O host layer as stated already. Consequently, the electro-

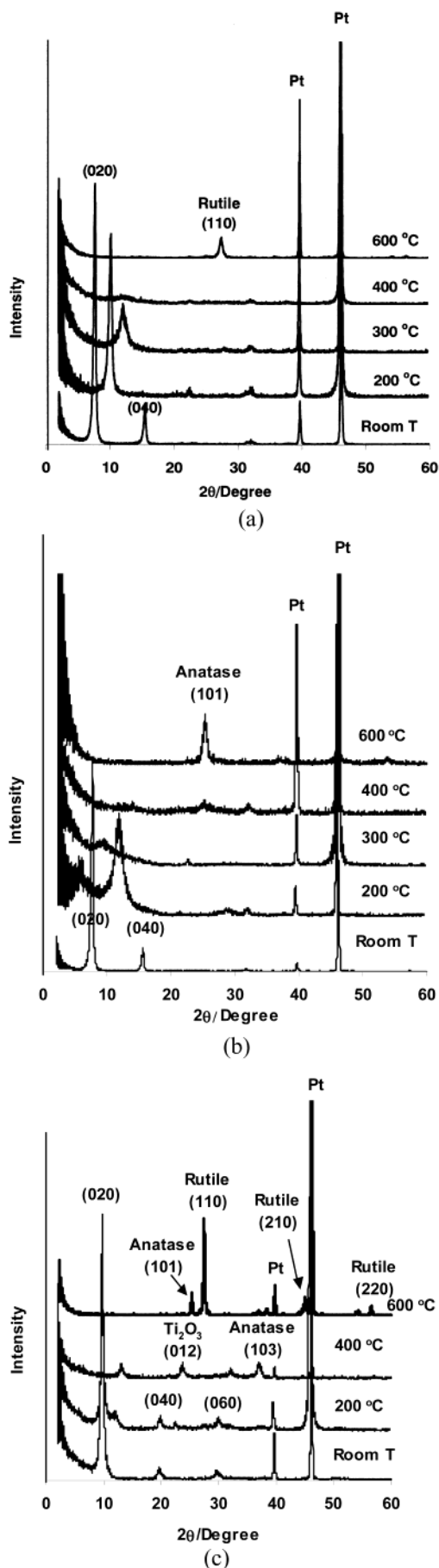


Figure 7. The XRD patterns of the (a) $\text{Ru}(\text{NH}_3)_6^{3+}$, (b) $\text{Co}(\text{NH}_3)_6^{3+}$, and (c) $\text{Ag}(\text{NH}_3)_2^+$ intercalated films at different temperatures.

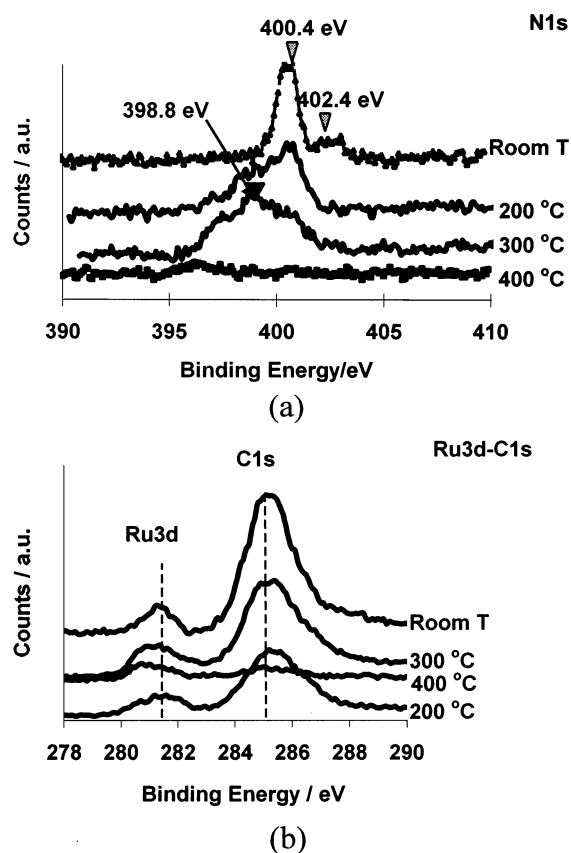


Figure 8. XPS (a) N1s and (b) Ru3d spectra of the $\text{Ru}(\text{bpy})_3^{2+}$ intercalated oxides heated at different temperatures.

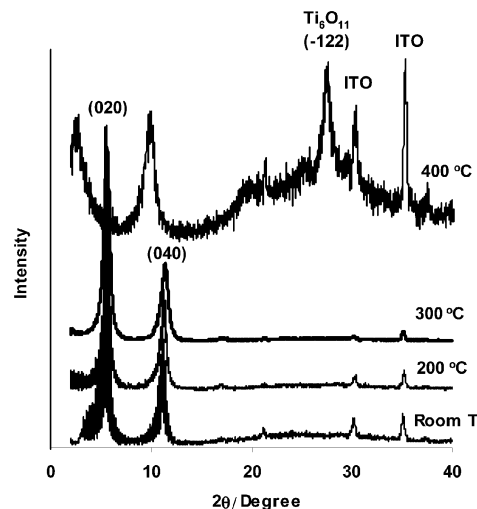


Figure 9. XRD pattern of the $\text{Ru}(\text{bpy})_3^{2+}$ intercalated oxide heated at different temperatures.

chemical measurements of all of the intercalated samples were carried out immediately after the immersion into the electrolyte saturated with N_2 .

The redox reactions of the intercalated complex cations were observed for samples intercalated with both the $\text{Ru}(\text{bpy})_3^{2+}$ (nonheated) and $\text{Ag}(\text{NH}_3)_2^+$ but not for the other samples as stated below. This difference is based on the degree of the interaction of the complex with the Ti—O host layer. In the case of the $\text{Ru}(\text{bpy})_3^{2+}$ intercalated sample, a charge-transfer bridge will exist because of the weakly interacted pyridine/Ti—O host layer and strongly interacted Ru^{2+} /pyridine couples. The $\text{Ag}(\text{NH}_3)_2^+$ intercalated sample exhibits a direct interaction of

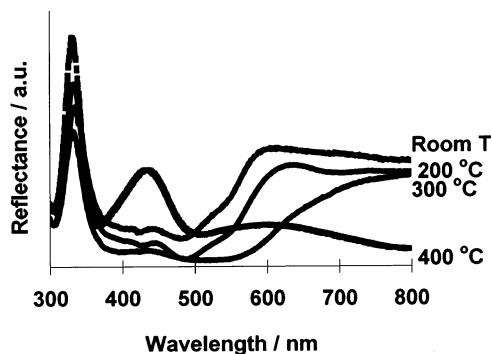


Figure 10. UV-vis reflectance spectra of the $\text{Ru}(\text{bpy})_3^{2+}$ intercalated oxides heated at different temperatures.

$\text{Ag}/\text{Ti}-\text{O}$ host layer couple. Therefore, the redox reactions of the intercalated complex cations will occur for these samples because the electron transfer easily takes place through the $\text{Ti}-\text{O}$ host layers via the interactions such as a resonance tunneling. On the other hand, in the case of the hexaammine complex $[\text{M}(\text{NH}_3)_6^{n+}]$ intercalated samples, the NH_3 ligands surrounding the center M^{n+} suppress the direct interaction of the M^{n+} with the $\text{Ti}-\text{O}$ host layer, and interactions of both the $\text{NH}_3/\text{Ti}-\text{O}$ and $\text{M}^{n+}/\text{NH}_3$ are too weak to transfer the electron.

The cyclic voltammograms, which were performed under illumination (light on/off) in 0.1 M K_2SO_4 solution, of the $\text{Ru}(\text{bpy})_3^{2+}$ intercalated films nonheated and heated at 300 °C are given in the Figure 11, panels a and b, respectively. The redox peaks due to the $\text{Ru}(\text{II})/\text{Ru}(\text{III})$ couple for the $\text{Ru}(\text{bpy})_3^{2+}$ complex were observed in the region from 1 to 1.2 V (vs Ag/AgCl) for the nonheated sample. The observed anodic photocurrent after the oxidation to the $\text{Ru}(\text{III})$ state is due to the hole produced in the $\text{Ti}-\text{O}$ host layers under UV illumination. The photocurrent was also produced under visible light in the same region, but it was very low (see Supporting Information, Figure S4). However, only low photocurrents were observed in the potential region of $\text{Ru}(\text{II})$. (The large anodic photocurrent has been developed from around 0.5 V for the $\text{Cs}_x\text{Ti}_{(2-x/4)}\text{O}_{(4-x/4)}$).³⁵ These phenomena mean that $\text{Ru}(\text{II})$ acts as the recombination center between the excited electron and hole in the $\text{Ti}-\text{O}$ host layer, but $\text{Ru}(\text{III})$ does not. All of the transition metal complex cations, excluding $\text{Ru}(\text{III})$, used in this study acted as the recombination center. The redox reaction must accompany an intercalation/release of the solution cations (H_3O^+ or K^+ or both) in the interlayer because the system has to keep the neutrality of the layered oxide during the electrochemical reaction. The reaction mechanism is illustrated in Figure 13a.

On the other hand, no redox reaction was observed for the $\text{Ru}(\text{bpy})_3^{2+}$ intercalated sample heated at 300 °C, for which no deintercalation of the $\text{Ru}(\text{bpy})_3^{2+}$ occurred. However, it should be noted that the heated sample exhibited both anodic and cathodic photocurrents even under visible light illumination in which the light with a wavelength shorter than 420 nm was cut by a cutoff filter. The visible photoresponse is in harmony with the result obtained from the UV-vis spectra in Figure 10. The $\text{Ru}(\text{bpy})_3^{2+}$ molecule in the layer absorbs the visible light and is excited to its MLCT state to form $\text{Ru}(\text{bpy})_3^{2+*}$, which leads to the photocurrent. The changing potential from the cathodic to the anodic photocurrent is in the range from 0.3 to 0.6 V (two arrows in the figure), which corresponds to the flatband potential of the sample. The behavior of the system under the illumination is illustrated in Figure 13b, where the conduction band (CB) edge of the sample is assumed to be positioned at 0.1–0.2 eV above the equilibrium hydrogen potential.³⁵ Electrons produced by the excitation from the HOMO level to the

LUMO level of the $\text{Ru}(\text{bpy})_3^{2+}$ under irradiation will go into the conduction band (CB) level of the $\text{Ti}-\text{O}$ host layers and will move through the CB levels. On the other hand, the produced hole will also move by the tunneling mechanism, in which the hole or electron moves through the LUMO levels. The cathodic and anodic photoelectrochemical reactions will result in the H_2 and O_2 evolution, respectively, according to the energy positions.

The $\text{Ag}(\text{NH}_3)_2^+$ intercalated oxide exhibited no deintercalation and some distinct behavior of the large redox current in the electrochemical measurements. The cyclic voltammograms of the $\text{Ag}(\text{NH}_3)_2^+$ intercalated sample in the dark are given in Figure 12a. As seen from Figure 12a, the system underwent an irreversible reduction of the interlayer silver complex molecules to Ag metal in the first cycle and then possessed only reversible $\text{Ag}/\text{Ag}_2\text{O}$ redox reaction in the following cycles according to the equilibrium potentials, where the $\text{Ag}(\text{NH}_3)_2^+/\text{Ag}$ equilibrium potential is a little more negative than that of the $\text{Ag}_2\text{O}/\text{Ag}$. In fact, the amount of N in the sample drastically decreased after the electrochemical measurement according to the XPS analysis. After the electrode was illuminated as seen in Figure 12b, the system still exhibited the redox reaction, but the electrode developed a small photocurrent in the first cathodic sweep. The electrode color changed from white to silver after the first cycle, which indicates the formation of the coarse Ag metal particulates by the illumination of UV light. The SEM micrograph taken after the cyclic voltammogram exhibited no significant change in the morphology of the film. In the case of the second cycle under illumination (after the electrode color changed to silver), the photocurrent disappeared. The reason for the observed photoresponse of the film before color change at the first cycle is the low-enough aggregation level of the silver metal atoms by reduction. That is, the photoresponse is due to the formation of the atomic or nanolevel Ag metal in the interlayer, while the coarse Ag metal particulates formed in the interlayer bring about no photoresponse. The formation of the Ag metal clusters by aggregation of the atomic or nanolevel Ag is photoassisted in the interlayer in the presence of TiO_6 layers and UV light.⁴⁴ The dependency of the photocurrent on the amount of silver in different systems has been reported in previous studies.^{44,45} The above electrochemical reactions also accompanied the K^+ intercalation/release to keep the neutrality of the sample during the electrochemical reaction because K^+ was detected in the sample after the electrochemical measurements.

Summary

In this study, we have represented a new technique to prepare intercalated titanate with a layered structure by using titanate nanosheets. When negatively charged $\text{Ti}-\text{O}$ nanosheets come into contact with complex cations, they combine to form the $\text{Ti}-\text{O}$ layered oxides intercalated with the complex cations due to the electrostatic self-assembly deposition (ESD) mechanism. The type of cation determines the stability of the intercalated layered oxides under heat treatment. For the ammine complexes, heat treatment brought about the decrease in the interlayer distance by the release of intercalated water. Further heat treatment resulted in the formation of the subsequent anatase and rutile phases depending on the kind of complex. In contrast with the ammine complex intercalated $\text{Ti}-\text{O}$ oxides, the $\text{Ru}(\text{bpy})_3^{2+}$ intercalated sample kept its layered structure without any change until 400 °C. In electrochemical measurements, both $\text{Ru}(\text{bpy})_3^{2+}$ and $\text{Ag}(\text{NH}_3)_2^+$ intercalated samples, for which some interactions between the complex cations and $\text{Ti}-\text{O}$ layer are present, showed the redox reactions together with the intercala-

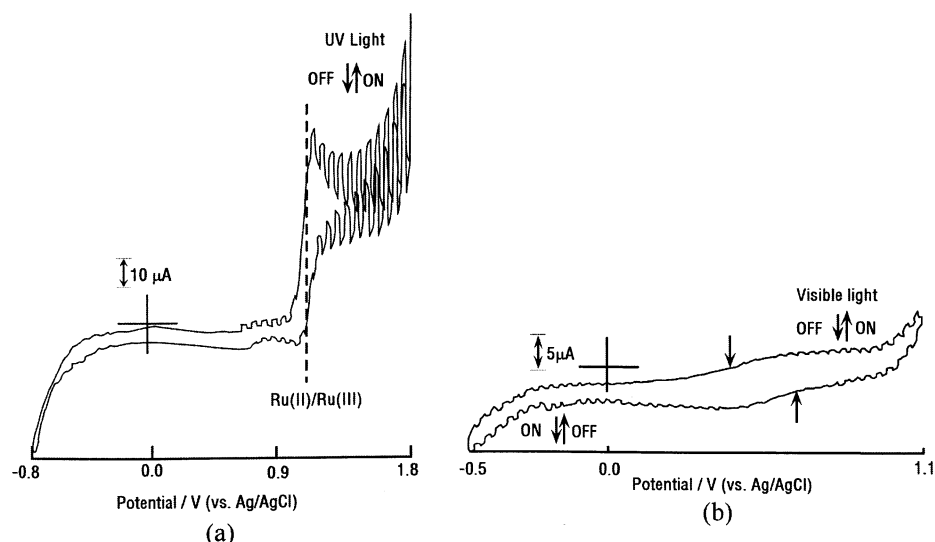


Figure 11. Cyclic voltammograms of the $\text{Ru}(\text{bpy})_3^{2+}$ intercalated oxides: (a) nonheated; (b) heat-treated at 300 °C. The arrows in panel b denote the changing potentials from anodic to cathodic photocurrents.

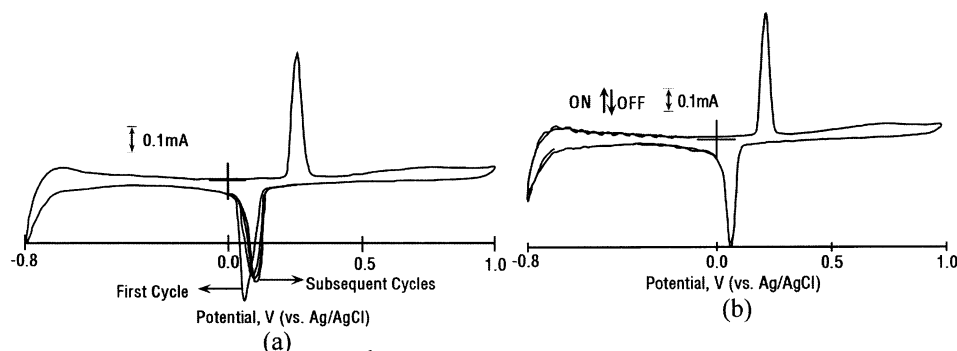


Figure 12. Cyclic voltammogram of the silver complex intercalated film under (a) no illumination and (b) illumination in UV light region.

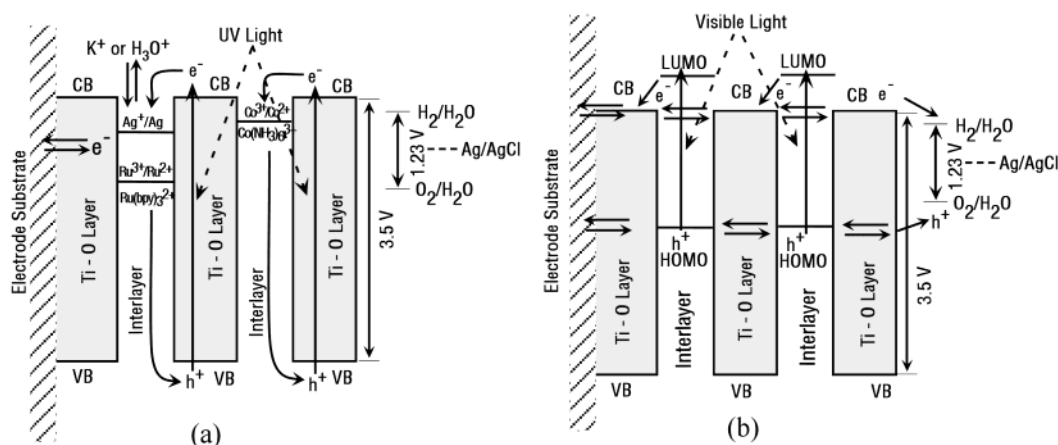


Figure 13. Possible mechanisms for the behavior of the complex cation intercalated oxides: (a) the redox reactions of the $\text{Ru}(\text{bpy})_3^{2+}$ and $\text{Ag}(\text{NH}_3)_2^+$ intercalated oxides and the recombination processes; (b) anodic and cathodic photocurrents of the $\text{Ru}(\text{bpy})_3^{2+}$ intercalated oxide heated at 300 °C.

tion/release reactions of the solution cations such as K^+ and H_3O^+ . For these samples, a tunneling mechanism through the Ti–O host layers was proposed. Simultaneously, the intercalated transition metal complexes acted as the recombination centers for the electron/hole pair produced in the Ti–O host layers under UV illumination. The $\text{Ru}(\text{bpy})_3^{2+}$ intercalated film heated at 300 °C, for which relatively strong interaction of the pyridine/Ti–O host layer is formed, showed the visible light photocurrent due to the excitation mechanism of the electrons from the HOMO to the LUMO levels of the $\text{Ru}(\text{bpy})_3^{2+}$. The silver complex

intercalated sample showed some distinct behavior. Potential sweep brought about the reduction of the interlayer complex cations to silver metal at a potential region more negative than about 0.2 V, and the photoresponse was also observed for this sample intercalated with the fine Ag metal particulates.

Acknowledgment. This work was supported by the Core Research for Evolutional Science and Technology (CREST) program of the Japan Science and Technology Co. (JST) and a

Grant-in-Aid for Scientific Research (Grant No. 15350123) from the Ministry of Education, Culture, Sports, Science, and Technology.

Supporting Information Available: The FTIR spectra of the ammine complex intercalated films (S1) and Ru(bpy)₃²⁺ intercalated films at different temperatures (S2), XRD patterns of the as-prepared Ru(bpy)₃²⁺ intercalated film before and after holding for 40 min in K₂SO₄ solution and the heat-treated film at 300 °C after 2 h of potential sweep (S3), and cyclic voltammogram of the nonheated Ru(bpy)₃²⁺ intercalated oxide under visible light illumination (S4). This material is available free of charge via the Internet at <http://pubs.acs.org>.

References and Notes

- (1) Unal, U.; Matsuo, D.; Matsumoto, Y.; Koinuma, M. *J. Mater. Res.* **2002**, *17*(10), 2644.
- (2) Airolidi, C.; Nunes, L. M.; de Farias, R. F. *Mater. Res. Bull.* **2000**, *35*, 2081.
- (3) Sasaki, T.; Izumi, F.; Watanabe, M. *Chem. Mater.* **1996**, *8*, 777.
- (4) Nakato, T.; Sakamoto, D.; Kuroda, K.; Kato, C. *Bull. Chem. Soc. Jpn.* **1992**, *65*, 322.
- (5) Yao, K.; Nishimura, S.; Imai, Y.; Wang, H.; Ma, T.; Abe, E.; Tateyama, H.; Yamagishi, A. *Langmuir* **2003**, *19*, 321.
- (6) Yao, K.; Nishimura, S.; Ma, T.; Okamoto, K.; Inoue, K.; Abe, E.; Tateyama, H.; Yamagishi, A. *J. Electroanal. Chem.* **2001**, *510*, 144.
- (7) Tong, Z.; Shichi, T.; Oshika, K.; Takagi, K. *Chem. Lett.* **2002**, 876.
- (8) Sasaki, T.; Komatsu, Y.; Fujiki, Y. *Chem. Mater.* **1992**, *4*, 894.
- (9) Sasaki, T.; Watanabe, M.; Komatsu, Y.; Fujiki, Y. *Inorg. Chem.* **1985**, *24*, 2265.
- (10) Abe, R.; Ikeda, S.; Kondo, J. N.; Hara, M.; Domen, K. *Thin Solid Films* **1999**, *343–344*, 156.
- (11) Sasaki, T.; Watanabe, M.; Michiue, Y.; Komatsu, Y.; Izumi, F.; Takenouchi, S. *Chem. Mater.* **1995**, *7*, 1001.
- (12) Sasaki, T.; Komatsu, Y.; Fujiki, Y. *Inorg. Chem.* **1989**, *28*, 2776.
- (13) Sumida, T.; Takahara, Y.; Abe, R.; Hara, M.; Kondo, J. N.; Domen, K.; Kakihana, M.; Yoshimura, M. *Phys. Chem. Chem. Phys.* **2001**, *3*, 640.
- (14) Nunes, L. M.; de Souza, A. G.; de Farias, R. F. *J. Alloys Compd.* **2001**, *319*, 94.
- (15) Abe, R.; Hara, M.; Kondo, J. N.; Domen, K.; Shinohara, K.; Tanaka, A. *Chem. Mater.* **1998**, *10*, 1647.
- (16) Abe, R.; Kondo, J. N.; Hara, M.; Domen, K. *Supramol. Sci.* **1998**, *5*, 229.
- (17) Choy, J. H.; Lee, H. C.; Jung, H.; Kim, H.; Boo, H. *Chem. Mater.* **2002**, *14*, 2486.
- (18) Choy, J. H.; Lee, H. C.; Jung, H.; Hwang, S. J. *J. Mater. Chem.* **2001**, *11*, 2232.
- (19) Yanagisawa, M.; Sato, T. *Solid State Ionics* **2001**, *141–142*, 575.
- (20) Cheng, S.; Wang, T. C. *Inorg. Chem.* **1989**, *28*, 1283.
- (21) Kooli, F.; Sasaki, T.; Watanabe, M.; Martin, C.; Rives, V. *Langmuir* **1999**, *15*, 1090.
- (22) Kooli, F.; Sasaki, T.; Watanabe, M. *Microporous Mesoporous Mater.* **1999**, *28*, 495.
- (23) Kudo, A.; Sayama, K.; Tanaka, A.; Asakura, K.; Domen, K.; Maruya, T.; Onishi, T. *J. Catal.* **1989**, *120*, 337.
- (24) Sayama, K.; Arakawa, H.; Domen, K. *Catal. Today* **1996**, *28*, 175.
- (25) Sayama, K.; Tanaka, A.; Domen, K.; Maruya, K.; Onishi, T. *J. Catal.* **1990**, *124*, 541.
- (26) Ohtani, B.; Ikeda, S.; Nakayama, H.; Nishimoto, S. *Phys. Chem. Chem. Phys.* **2000**, *2*, 5308.
- (27) Ikeda, S.; Tanaka, A.; Shinohara, K.; Hara, M.; Kondo, J. N.; Maruya, K.; Domen, K. *Microporous Mater.* **1997**, *9*, 253.
- (28) Harada, M.; Sasaki, T.; Ebina, Y.; Watanabe, M. *J. Photochem. Photobiol., A* **2002**, *148*, 273.
- (29) Kim, Y. I.; Samer, S.; Huq, M. J.; Mallouk, T. E. *J. Am. Chem. Soc.* **1991**, *113*, 9561.
- (30) Constantino, V. R. L.; Bizeto, M. A.; Brito, H. F. *J. Alloys Compd.* **1998**, *278*, 142.
- (31) Kudo, A.; Sakata, T. *J. Phys. Chem.* **1996**, *100*, 17323.
- (32) Kudo, A.; Kaneko, E. *Microporous Mesoporous Mater.* **1998**, *21*, 615.
- (33) Kudo, A.; Kaneko, E. *Chem. Commun.* **1997**, 349.
- (34) Kudo, A.; Kondo, T. *J. Mater. Chem.* **1997**, *7* (5), 777.
- (35) Matsumoto, Y.; Funatsu, A.; Matsuo, D.; Unal, U.; Ozawa, K. *J. Phys. Chem. B* **2001**, *105* (44), 10893.
- (36) Koinuma, M.; Seki, H.; Matsumoto, Y. *J. Electroanal. Chem.* **2002**, *531*, 81.
- (37) Abe, R.; Shinohara, K.; Tanaka, A.; Hara, M.; Kondo, J. N.; Domen, K. *Chem. Mater.* **1998**, *10*, 329.
- (38) Takata, T.; Furumi, Y.; Shinohara, K.; Tanaka, A.; Hara, M.; Kondo, J. N.; Domen, K. *Chem. Mater.* **1997**, *9*, 1063.
- (39) Pearce, J. R.; Gustafson, B. L.; Lunsford, J. H. *Inorg. Chem.* **1981**, *20*, 2957.
- (40) Omberg, K. M.; Schoonover, J. R.; Treadway, J. A.; Leasure, R. M.; Dyer, R. B.; Meyer, T. J. *J. Am. Chem. Soc.* **1997**, *119*, 7013.
- (41) Bossmann, S. H.; Turro, C.; Schnabel, C.; Pokhrel, M. R.; Payawan, L. M., Jr.; Baumeister, B.; Wörner, M. *J. Phys. Chem. B* **2001**, *105*, 5374.
- (42) Nakato, T.; Kusunoki, K.; Yoshizawa, K.; Kuroda, K.; Masao, K. *J. Phys. Chem.* **1995**, *99*, 17896.
- (43) Pels, J. R.; Kapteijn, F.; Moulijn, J. A.; Zhu, Q.; Thomas, K. M. *Carbon* **1995**, *33* (11), 1641.
- (44) Vamathevan, V.; Tse, H.; Amal, R.; Low, G.; McEvoy, S. *Catal. Today* **2001**, *68*, 201.
- (45) Wen, C.; Ishikawa, K.; Kishima, M.; Yamada, K. *Sol. Energy Mater. Sol. Cells* **2000**, *61*, 339.